Unveiling the impact of embedding resins on the physicochemical traits of wood cell walls with subcellular functional probing

Raphaël Coste, Mikhael Soliman, Nicolas Bercu, Sylvain Potiron, Karima Lasri, Véronique Aguié-Béghin, Laurene Tetard, Brigitte Chabbert, Michaël Molinari

Unveiling the impact of embedding resins on the physicochemical traits of wood cell walls with subcellular functional probing

Raphaël Coste [a,b,c], Mikhael Soliman [c], Nicolas B. Bercu [b], Sylvain Potiron [b], Karima Lasri [c], Véronique Aguié-Béghin [a], Laurene Tetard [c,d], Brigitte Chabbert [a], and Michaël Molinari [e]*

[a] Université de Reims Champagne Ardenne, INRA, FARE, UMR A 614, 51097 Reims, France.

[b] Université de Reims Champagne Ardenne, LRN EA 4682, 51097 Reims, France.

[c] NanoScience Technology Center, University of Central Florida, Orlando, Florida 32826, USA.

[d] Physics Department, University of Central Florida, Orlando, Florida 32816, USA.

[e] CBMN UMR CNR 5248, University of Bordeaux, IPB, Pessac, 33600, France.

Abstract

As pressing needs for exploring molecular interactions in plants soar, conventional sample preparation methods come into question. Though resins used to embed plant tissues have long been assumed to bear no palpable effect on their properties, discrepancies in recent studies exploiting nanoscale microscopy suggest that their impact could be significant at small scales. By juxtaposing the traits of poplar sections prepared with and without embedding, we evaluate the diffusion (penetration depth) of acrylic and epoxy resins commonly used for embedding. Our results unveil critical quantitative differences when probing mechanical properties with a microscale nanoindentation indenter or a nanoscale tip. The latter resolves significant stiffness variations between the compound middle lamellae, the secondary cell wall layers S1 and S2, and the cell corner, not accessible with nanoindentation. Similar observations are drawn from comparing confocal Raman and nanoscale infrared spectroscopy. Our findings shed light on the effect of resin diffusion suggesting acrylic LR White to be the least diffusive for plant cell wall studies.

Keywords

Natural Fibres (A); Mechanical properties (B); Atomic Force Microscopy (D); Infrared (IR) spectroscopy (D); Raman spectroscopy (D).

1. Introduction

Lignocellulosic (LC) biomass represents a promising renewable resource to contribute to the global demand for sustainable production of energy, chemicals, textiles and eco-friendly materials [1, 2]. The rich prospects lay in the properties of plant fibres, mainly composed of carbon-rich materials cellulose, hemicelluloses and lignin. Plant cell walls feature a multi-layered organization with mixtures of the three aforementioned constituents organized into functional layers. The matrices constitutive of the cell corner (CC), the compound middle lamella (CML) (association of the middle lamella and the primary wall) and the secondary cell wall layers (S1, S2, and S3) can be thought of as nanocomposites consisting of an amorphous matrix of varying concentration of hemicelluloses, pectins and lignin reinforced by semi-crystalline cellulose microfibrils. The structure, morphology and composition of plant systems depend on their botanic origin, environmental and developing conditions [3]. Based on such cell wall layer heterogeneities, the effectiveness of chemical treatments associated with processing LC biomass for various applications can be very poor, such as in the case of biomass deconstruction for biofuel production. The complexity of the multi-layered tissues and the paucity of tools available to understand the native properties of plants without interferences from sample preparation further hinder advances in this field [4, 5].

Characterizing intact plant tissues has been reported in several studies with different analytical techniques including Raman spectroscopy [6, 7], Fourier Transform Infrared (FTIR) spectroscopy [8, 9], Nuclear Magnetic Resonance (NMR) [10], nanoindentation [11, 12] or AFM-IR [13, 14]. However, when it comes to measuring the mechanical properties of plant cell walls at the nanoscale, the surface of the sample has to display very low roughness. This is challenging to obtain without embedding of plant tissues. This process generally involves chemical fixation including alcoholic dehydration, resin embedding and surface preparation with microtome sectioning [15]. Until recently, the hypothesis that the aforesaid steps maintain the plant cells in a near native state had been mostly unchallenged [16, 17]. However, mechanical studies of plant cell walls of non-embedded and embedded wood tissues at the

micro- and nanoscales increasingly suggest that resin embedding processes can impair their mechanical properties [18-20], even leading to contradictory results [21, 22]. Thus, it is becoming clear that resin penetration in plant tissues constitutes a complex process that should be studied both structurally and chemically at the sub-cellular level. Overall, to date, traditional analytical methods available to study the effects of resin diffusion in plant tissues did not offer sufficient spatial resolution nor the necessary sensitivity to detect variations in physicochemical properties within cell wall layers. Moreover, the extent to which the volume probed by different methods affects the results has not yet been evaluated. Our present work tackles this pending issue by comparing the impact of three resins, namely Epon, LR White and Methacrylate, on the mechanical properties of poplar cell wall layers at micro- and nano-scales. While Epon and LR White represent common embedding resins, Methacrylate is considered here to evaluate the benefit of a potential washing step following specimen embedding and sectioning. Poplar was used as a model system because of its mechanical strength, allowing for sectioning of intact cell walls with low roughness, which is critical to make nanoscale characterization possible. The intact non-embedded sections constitute a control for the study. At the microscale, nanoindentation and Raman spectroscopy are used to study the mechanical properties and composition of the secondary layers (S2), respectively. As the heterogeneities within the cell walls involved smaller volumes than what nanoindentation and Raman spectroscopy can resolve, finer details of the properties variations are explored with nanoscale capabilities including Atomic Force Microscopy (AFM), PeakForce Quantitative Nanomechanical property Mapping (PFQNM) [23, 24] and nanoinfrared (nanoIR) AFM [25]. These techniques reveal local mechanical and molecular changes in S1 and S2 layers, as well as in CML and CC of wood cell walls [13, 23].

2. Experimental

2.1. Plant material

Small portions of about 6mm x 5mm x 3mm (longitudinal x tangential x radial) were sectioned from stems of three-year old poplar (Populus tremula x Populus alba, grown in greenhouse) with a stainless

steel razor blade. Sections to be embedded in resin were dehydrated in an ethanol series (25%, 50%, 70%, 80%, 95% and 100%) while the non-embedded samples were not treated at all, considering that the dehydration is part of the embedding process. For Epon embedding, samples were dehydrated with acetone following the ethanol series, before being soaked in ethanol/resin solutions with an increasing ratio of resin up to 100%. Between each step, the sections were placed in a desiccator under vacuum for 15min to remove air bubbles inside the cell lumen. Samples were finally cured in specific gelatin capsules at 37°C for 24h followed by 60°C for 48h. For LR White and Methacrylate, samples were soaked in ethanol/resin solutions with an increasing ratio of resin up to 100% immediately after ethanol dehydration. The final step in gelatin capsule was done at 60°C for 24h. An additional set of samples initially embedded in Methacrylate was washed in successive baths of acetone that were changed every 3min for 90min under low speed agitation on an orbital shaker.

2.2. Plant material sectioning

For nanoindentation measurements, blocks of 2mm were prepared by cutting the bottom of the resin block with a small saw, leaving the top surface sectioned with the diamond knife untouched for measurements. The bottom of the block was then flattened with fine sand paper to ensure a proper attachment with the substrate. The 2mm blocks were well adhered onto Si/SiO_2 substrates using double sided adhesive. For the other measurements, the samples were cut using a glass knife mounted on a HM 360 Microm Microtech microtome. For all the experiments including nanoindentation, the side to be analyzed was submitted to a second surfacing with a high grade diamond knife (AFM grade) to obtain a roughness below 50nm, which is required to avoid measurement artefacts during nanoscale imaging and spectroscopy. For all mechanical measurements (nanoindentation and AFM PFQNM), special care was taken to ensure that the samples were well adhering to the substrate to avoid artifacts from adhesion issues (Jakes, 2011) [26]. The back sides of the samples used for nanoindentation were flattened with fine sand paper while the thin sections of 2µm used for AFM PFQNM as well as for Raman measurements were directly obtained by microtoming with the diamond knife. The monitoring of the

force curves during AFM analysis confirmed the stability of the adhesion of the section on the substrate during the experiments. For nanoIR spectroscopy, thinner cross sections of 500nm were placed on ZnSe substrates and well adhered through capillary adhesion, to limit the contribution of the volume of the sample in the photothermal expansion measured by the AFM tip. To obtain 500nm thick non-embedded poplar section, blocks of 3cm x 1cm x 1cm (longitudinal x tangential x radial) were sectioned from the stem and one extremity was cut into a pyramidal shape to facilitate micro-sectioning. The area was softened with ultrapure water using a cotton swab to obtain 500nm sections using a diamond knife.

2.3. Micromechanical analysis with Nanoindentation

Nanoindentation measurements were carried out on a Triboscope (Hysitron Inc.) coupled to a Nanoscope II (Digital Instruments) following commonly used method [27]. The Triboscope was equipped with a Berkovich indenter of radius around 400nm determined by scanning electron microscopy (SEM). Reported values of reduced indentation modulus (IM), also called reduced Young's Modulus, correspond to an average of 5 curves collected on three different cells. Dimensions of the indenter restricted the probing to the S2 layers. The cycle consisted of a load ramp lasting 15s (load rate 33.33µN/s) followed by a holding segment at maximum load of 500µN for 10s, before unloading (load rate 33.33µN/s) to reach 10% of the maximum load. A final holding segment was carried out to take into account thermal drift. Reduced IM was calculated using the Oliver and Pharr model [28]. All experiments were conducted in ambient air with a relative humidity at 35% ± 5% and a temperature of 20°C.

2.4. Nanomechanical analysis with PFQNM

PFQNM measurements were conducted on a Multimode 8 AFM (Bruker, USA) using cantilevers with nominal spring constants of 200N/m (RTESPA-525) selected according to the reported literature on similar samples [23]. The deflection sensitivity of each probe was calibrated before use by carrying out indentation ramps on a clean and hard (Esapphire~450GPa) sapphire surface. The average of three measurements was used for analysis. AFM tip radii (20-50nm) were determined before and after

experiments using a reference titanium roughness sample (Bruker, USA). Cantilever spring constants, also measured before and after each experiment, were calculated following the Sader method [29]. All measurements were conducted in ambient air with a relative humidity at 35% ± 5% and a temperature of 20°C. After collecting PFQNM force-distance curves in the desired area, the data was fitted to extract the reduced IM using the conventional Derjaguin-Muller-Toporov (DMT) model [30]. DMT model was identified as the best suited model according to experimental parameters, tip geometry, and the properties of the plant cell walls. The force curves were subjected to baseline correction when needed and any variations in the tip radius and the cantilever spring constant that could occur during measurements were not significant after one sample scan. This is included into the standard deviation of the reduced IM. Reported values of IM correspond to an average of 10,000 force curves for the S2 layer, 4,000 force curves for the CC, 2,000 force curves for the S1 layers and 1,000 force curves for the CML. Measurements were collected over 2 adjacent cells. At least five areas were scanned on different samples prepared with the same Poplar fibre. As it is known that the indentation modulus variations could be due to topography effects, great care was taken to confirm the absence of correlation between the topography and the nanomechanical map. Particularly, because of the low roughness of the different samples (<50nm), which is even lower in any given sub-layer (inferior to 15nm), the variations in IM was attributed to the effect of resin embedding.

2.5. Chemical analysis at the microscale with Raman microscopy

Raman measurements were performed on a WITec alpha 300 RA confocal Raman system equipped with Zeiss 100X objective, and a spectrometer with a 600gr/mm grating and CCD camera detector. The samples were excited with 532nm laser light (~ 200µW) in ambient air with a relative humidity at 35% ± 5% and at a temperature of 20°C. The spectra were collected using an integration time of 0.5s in different regions of each sample to take into account the natural variability of the samples. All spectra were processed with using cosmic ray removal (CRR), background subtracting (polynomial) and Savitzky-Golay smoothing.

2.6. Chemical analysis at the nanoscale with nanoIR

Nanoscale infrared spectroscopy and chemical maps were collected on a nanoIR2 (Bruker, Santa Barbara, USA) using a pulsed infrared laser (optical parametric oscillator (OPO) or quantum cascade laser (QCL)) to excite the samples mounted on a transparent ZnSe substrate. PR-EX-TNIR-A probes (Bruker, USA), with nominal spring constant of 0.4 N/m, were used. NanoIR spectra were collected using the 1800 to 1000cm^{-1} wavelength range of the OPO laser in ambient air with a relative humidity at 35% ± 5% and at a temperature of 20°C. As specific energies corresponding to the vibrational modes of the biopolymers in poplar are absorbed, heat is released to the lattice giving rise to local photothermal expansion. The pulsed nature of the excitation sets the cantilever, in contact with the surface, into oscillation (or ringing). By applying a Fast Fourier Transform (FFT) to the cantilever signal S(t) captured by the photodetector, the signal is represented in frequency space. Several peaks were observed in the FFT spectrum, which correspond to the contact resonance modes of the cantilever. The amplitude and frequency of the first mode were monitored as a function of illumination wavenumber. The resulting amplitude vs. wavenumber curve corresponds to a localized IR spectrum of the plant cell wall. Chemical maps were acquired by fixing the laser wavelength to match with one of the absorption band of the sample, and the pulse frequency of the laser to match the resonant contact mode.

3. Results

Nanoindentation is commonly used in mechanical measurements of fibres. In this study, it was considered to compare the reduced indentation modulus (IM) of non-embedded and embedded poplar cross sections (Fig. 1a). Due to the large radius of the indenter (around 400nm), S2 layers, with thickness in the range of 0.5-2.5µm, were the only regions that could repeatedly be probed without any interference from neighboring layers. The thickness of the CML (50-150nm) and the S1 layer (100-350nm) [23] far smaller than the diameter of the nanoindenter, prevented their inclusion in this part of the study. Reduced IM values were extracted from nanoindentation curves (Fig. 1b) for the S2 layers of each sample. Non-embedded poplar revealed a reduced IM of 14.5±0.6GPa (Fig. 1c), which is in

agreement with values of 16.9±1.9GPa and 17.4±1.4GPa previously reported by Wu et al. [31] and Zhang et al. [32] respectively. However a slight variation (~ 2.5-3GPa) in the average modulus compared to previous reports was observed, which could be due to biological variability, as the poplar tree used here was 3 years old, while Wu et al. [31] worked on 16 year-old poplar tissues (Populus spp.). Several parameters such as nearby edges in the sample [11, 26] and environmental conditions including relative humidity can also influence the measurements [33, 34]. Next, the impact of resins was investigated under identical experimental conditions. A significant increase of the reduced IM to 22.3±4.5GPa was found in S2 layers embedded with Epon, suggesting some diffusion in the cell wall. Pure Epon, probed as a reference, exhibited a reduced IM of 4.8±0.6GPa (Table 1). As a result, we infer that Epon reinforced the cell wall's modulus. The reduced IM of LR White and Methacrylate embedded sections showed different behaviors despite both pure resins being acrylic polymers with similar reduced IM of 4.7±0.6GPa and 4.5±0.4GPa, respectively (Table 1). LR White seemed to preserve the properties of native poplar with a reduced IM of 14.5±2.9GPa, which is close to the value of the non-embedded sample. The poplar specimen prepared with Methacrylate exhibited an important increase of IM to 21.9±4.9GPa. Interestingly, after washing Methacrylate (see Experimental section), a reduced IM close to that of non-embedded poplar could be retrieved. Based on the size of the Berkovich indenter, we estimated that nanoindentation measurements in S2 correspond to a deformation of 1.5-5.5μm^3 for an applied load of 500µN (Fig. 1a). In plant tissues, such a large indent involves the displacement of a very heterogeneous matrix made of cellulose, hemicellulose and lignin. Local variations occurring at the scale below 50nm laterally and below 10nm in depth would not lead to significant changes in the Berkovich indenter measurements, but would appear as a different indentation modulus when measured with the AFM cantilever in AFM PFQNM. If such a small volume was occupied by resin, AFM PFQNM would detect an indentation modulus close to that of the pure resin.

Hence, to explore the mechanical properties of the different cell layers with finer details, a nanomechanical technique more suitable for smaller volume indentation, AFM PFQNM, was used.

Given the dimension of the AFM tip diameter in the 20-50nm range, the volume probed was estimated in the 10^3-10^5nm^3 range depending on the load applied (Fig. 1a). With small load, the probing volume would allow for the differentiation of the S1, CML and CC regions of the cell walls in addition to the S2 layer. The values provided in Fig. 2 and Table 1 were obtained by carefully selecting regions with no sign of structural damage or uneven topography to avoid artefacts (see Fig. 2b and Supplementary Information).

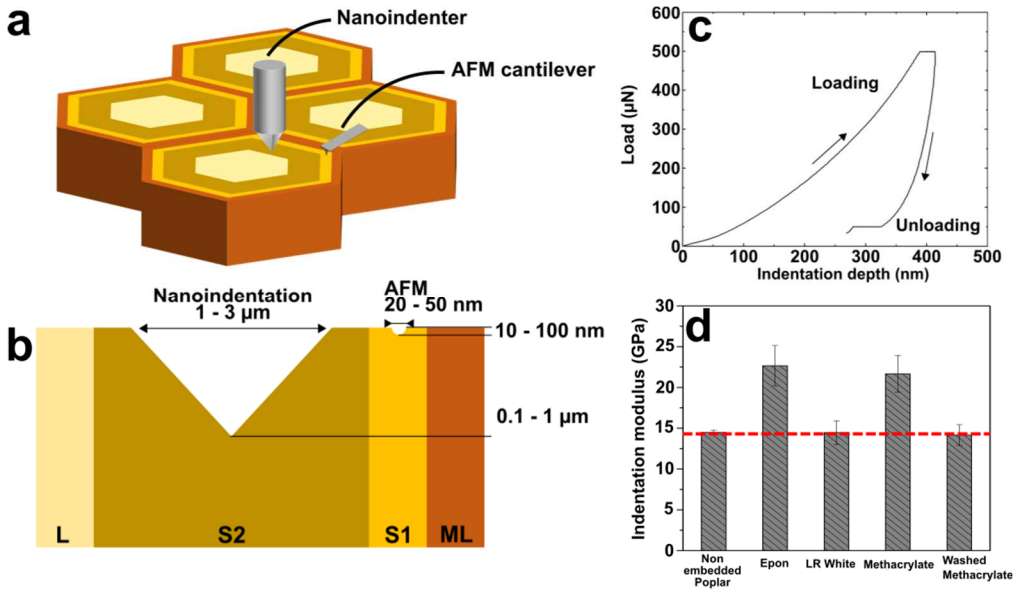

Figure 1. Mechanical properties of wood cell walls by nanoindentation and AFM measurements. (a) 3D representation of a wood plant cross section. The nanoindenter and AFM cantilever illustrate the difference in probe size. (b) Side section view of a plant cell wall section showing the different layers that compose the cell wall and illustrating the difference of volume probed with nanoindentation and AFM measurements. (c) Typical load versus indentation depth curve obtained by nanoindentation. (d) Histogram of reduced IM calculated in the S2 layers of poplar by nanoindentation. The measurements represent the values obtained for non-embedded poplar, poplar embedded in Epon, poplar embedded in LR-White, poplar embedded in Methacrylate, and poplar after washing Methacrylate. The dotted red line corresponds to the value of the reduced IM obtained for non-embedded poplar. Error bars correspond to the standard deviation.

For direct comparison, the results obtained by nanoindentation in the S2 layer are shown side-by-side in Table 1 and Fig. 2a. The IM of the S2 layer of the control obtained by PFQNM, 16.2±1.9GPa, was very similar to the nanoindentation result. Such similar values between nanoindentation and PFQNM have already been observed in other studies of hemp fibres [15]. We point out that the standard deviation of PFQNM data is much higher than that observed with nanoindentation, which highlights both the sensitivity of the method and confirms heterogeneities in the tight assemblies of biopolymers. As predicted, the lack of resolution of nanoindentation prevented from accessing fine details of the plant cell wall behavior.

Table 1. Reduced IM of the resins and poplar cell layers measured by nanoindentation and AFM PFQNM.

Resins	Nanoindentation reduced IM (GPa)	PFQNM reduced IM (GPa)			
Pure Epon	4.8 ± 0.6	5.4 ± 1.0			
Pure LR White	4.7 ± 0.6	4.5 ± 0.9			
Pure Methacrylate	4.5 ± 0.4	3.6 ± 0.7			
Plant sections	S2	S2	S1	CML	CC
Non-embedded poplar	14.5 ± 0.6	16.2 ± 1.9	15.6 ± 3.7	12.1 ± 2.0	11.4 ± 0.7
Poplar Epon	22.3 ± 4.5	23.9 ± 2.8	13.3 ± 1.9	12.5 ± 2.2	11.2 ± 1.4
Poplar LR White	14.5 ± 2.9	18.2 ± 3.5	16.0 ± 3.8	10.6 ± 1.0	10.8 ± 2.1
Poplar Methacrylate	21.9 ± 4.9	7.1 ± 1.0	5.0 ± 0.7	4.5 ± 0.4	4.8 ± 0.3
Poplar Washed Methacrylate	14.2 ± 2.6	27.3 ± 4.7	16.7 ± 2.4	13.8 ± 1.9	12.3 ± 0.5

Error values correspond to standard deviation.

The reduced IM for the S2 layers measured using PFQNM (Fig. 2) were higher than the ones obtained with nanoindentation for Epon and LR White (Table 1), while pure resins exhibited moduli similar to the ones obtained by nanoindentation, between 3.6GPa and 5.4GPa.

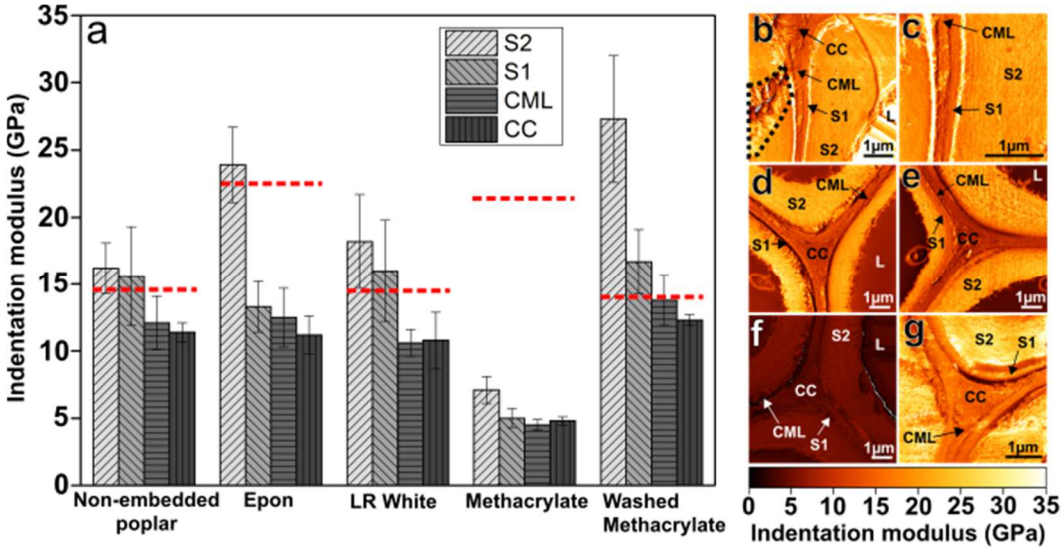

Figure 2. Mechanical properties of the cell wall layers by PFQNM. (a) Reduced IM obtained with PFQNM in the S2 layer (light grey), S1 layer (medium grey), CML (medium dark grey), and in the cell corner (CC) (dark grey). Red dotted lines correspond to the reduced IM obtained in the S2 layer with nanoindentation. Error bars correspond to standard deviation. (b-g) Reduced IM maps of the corresponding cross sections obtained for (b,c) non-embedded poplar, (d) poplar embedded in Epon, (e) poplar embedded in LR White, (f) poplar embedded in Methacrylate and (g) poplar after washing Methacrylate resin. The cell wall layers are labelled as L: lumen, S1: secondary S1 layer, S2: secondary S2 layer, CC: cell corner and CML: compound middle lamellae. The dotted line on the non-embedded poplar (Fig. 2b) highlights a damaged region of the cell wall discussed in SI. The error bars correspond to the standard deviation.

Epon-embedded poplar showed a significant increase in IM (23.9±2.8GPa) compared to the non-embedded sample (16.2±1.9GPa). For the section embedded in LR White, IM at 18.2±3.5GPa was the closest to the non-embedded control, though a larger standard deviation was observed. The standard deviation could be attributed to biological variability of the poplar from one sample/cell to the other but also to the non-uniform effect of the resin on the tissues. S2 embedded in Methacrylate had a noticeably lower IM at 7.1±1.0GPa, which increased to 27.3±4.7GPa after washing Methacrylate. This is in agreement with Muraille et al. that reported a reduced IM of 25.9±2.8GPa in the S2 layer of washed-Methacrylate poplar sections using PFQNM [23].

Variations of IM in the CC, S1 and S2 layers were also considered with PFQNM. The reduced IM of non-embedded poplar was found to be 15.6±3.7GPa in S1. Although to a lesser extent than the impact it had on S2, embedding poplar tissues in Epon affected the S1 layer (13.3±1.9GPa). LR White did not seem to impact S1 layers (16.0±3.8GPa). In the CML and the CC, all moduli remained similar to what was observed in the non-embedded poplar (12.1±2.0GPa in CML and 11.4±0.7GPa in CC), with 12.5±2.2GPa in CML and 11.2±1.4GPa in CC for Epon, and 10.6±1.0GPa in CML and10.8±2.1GPa in CC for LR White. For Methacrylate, the behavior was significantly different as the reduced IM measured in all layers were low: 7.5±1.0GPa in S2, 5.0±0.7GPa in S1, 4.5 ±0.3GPa in CML and 4.8±0.3GPa in CC. These values were very close to the pure resin (4.5 ± 0.4).

The washing process did not lead to full recovery of the IM, although the values for S1 and CC were closer to the control than the values of S2. Muraille et al. also observed a reduced IM of 17±1.4 GPa, 21.1±1.8 GPa in the CML and S1 layer of washed-Methacrylate poplar sections using PFQNM [23].

We probed the composition of the cell wall layers with Raman spectroscopy and nanoinfrared AFM (nanoIR) in an effort to better understand the interactions between resin and cell wall at the molecular level. Raman spectroscopy can be thought of as the chemical analysis counterpart of nanoindentation in this study, considering that the focal volume of a 100x objective in 300-500nm in diameter and about 1µm in depth. Thus, S2 was the only layer laterally sufficiently thick to be consistently studied without interference from the neighboring layers. Some cell corners could also be probed when their width was above 500nm. Raman experiments have been previously used to characterize wood cell walls [35, 36]. A typical Raman spectrum of S2 in non-embedded poplar (black curves in Fig. 3a-d) exhibited several bands attributed to cellulose (1095, 1120 and 1330cm^{-1}), hemicellulose (2935 and 1120cm^{-1}) and lignin (1601 and 1672cm^{-1}) (Table 2), in good agreement with the literature for plant fibres [35].

Raman spectra of S2 in poplar prepared with resins are shown in Fig. 3a-d, and compared with the spectra of pure resins. The characteristic bands of the resins are provided in Table S1 (SI). Some of the resin bands overlap with the poplar fingerprint, making it difficult to differentiate them. Nevertheless,

some undoubted differences could be identified. Although Raman spectra of embedded sections exhibited bands corresponding to cellulose, hemicellulose and lignin similar to raw poplar, some changes in band position and intensity could be noted. In presence of Epon, an increase in intensity of the 1460cm^{-1} band was observed. Spectra of the LR White-embedded poplar indicate the lowest concentration in resin, as confirmed in Fig. S1. In the case of Methacrylate embedding, bands characteristics of the resin clearly appeared in the spectra of the embedded sample.

Washing the resin led to retrieving Raman bands similar to the poplar fingerprint. Further investigation of resin diffusion was carried out by extracting chemical maps using a band corresponding to the resin, and found to be clearly different from the poplar signature. For all three resins, a band centered at 1724cm^{-1}, corresponding to C=O stretching, turned out to be suitable for chemical mapping. The resulting intensity maps for Epon, LR White, Methacrylate, and washed Methacrylate embedded poplar are shown in (Fig. 3e-h). The map of non-embedded poplar at 1724cm^{-1} is presented in SI. In addition to the lumen (L), Epon seemed to be homogeneously distributed in the cell wall while LR White in S2 appeared to be low. The signal corresponding to methacrylate was observed throughout the section before washing. After washing, the resin was removed from the lumen, residues were detected in a few cell regions. We note that the high signal in the CC appeared to be an artifact of a high fluorescence background in the region, but no band corresponding to the resin could be observed in the CC spectra (see Figures S3 and S4 in SI).

These observations were confirmed by a more quantitative correlation analysis (Fig. S1 and SI), which assessed the diffusion of the different resins within the lumen (L), S2 and CC of the poplar cell walls. Overall, the results are in agreement with the nanoindentation findings, suggesting that LR White diffuses the least in S2 compared to Methacrylate, which seems to cover the section.

Given the limited spatial resolution of Raman confocal spectroscopy, small residues of resins would not be resolved. Hence, nanoIR was used to explore the chemical properties of finer details previously revealed by PFQNM.

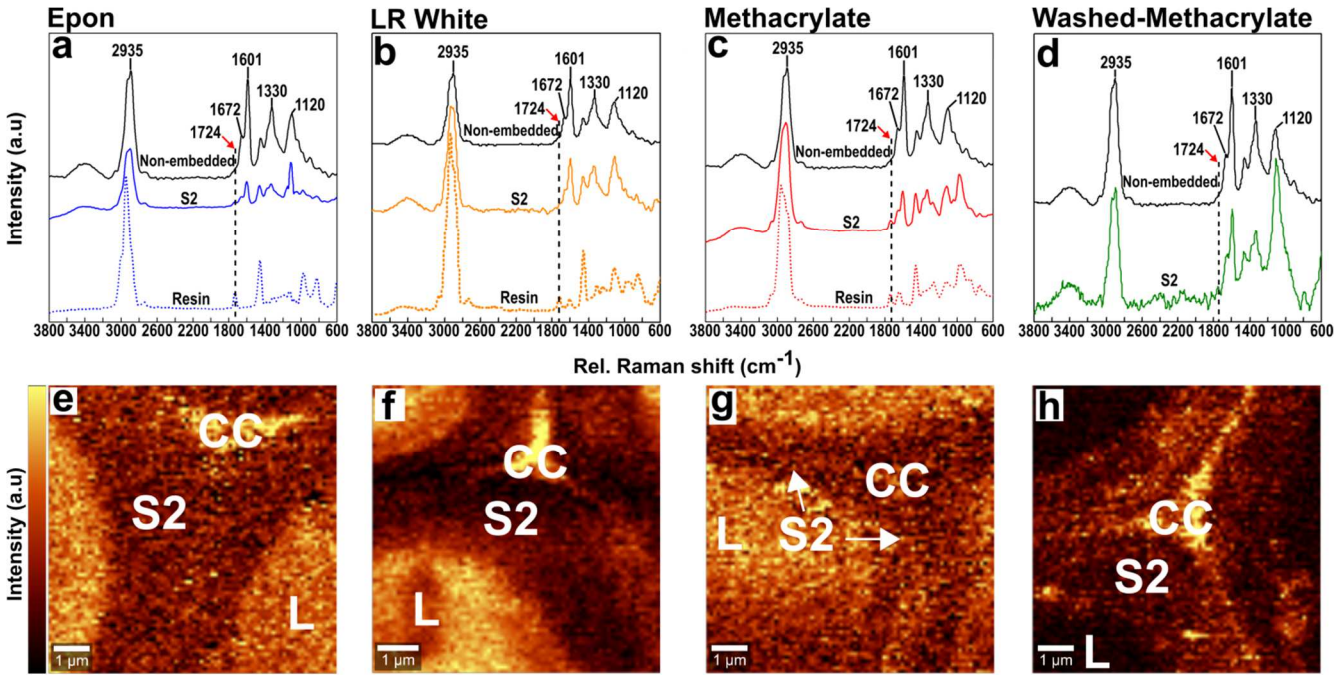

Figure 3. Confocal Raman spectroscopy of poplar wood cell walls (a-d) Raman spectra of S2 layer non-embedded poplar (black curve) along with (a) S2 layer poplar Epon (straight blue curve) and pure Epon (dotted blue curve); (b) S2 layer poplar LR White (straight orange curve) and pure LR White (dotted orange curve); (c) S2 layer poplar Methacrylate (Straight red curve) and pure Methacrylate (dotted red curve); (d) S2 layer poplar washed Methacrylate. (e-h) Raman chemical maps representative of the resin at 1724cm^{-1} for (e) poplar Epon, (f) poplar LR White, (g) poplar Methacrylate and (h) poplar after Methacrylate was washed.

NanoIR offers lateral resolution below 50nm [37], which makes the composition of S1, CML and CC accessible. After acquiring an AFM height image to determine the morphology of cell walls, the tip of the cantilever was positioned on the layer of interest to acquire an IR spectrum. This technology allows to get reliable spatially resolved chemical information. The bands revealed by high photothermal expansion were found to be similar to those obtained in conventional mid-infrared spectroscopy such as with FTIR spectroscopy [38]. However, we note that the band intensities and ratios obtained with nanoIR can be different than those reported in the literature for FTIR, due to the difference in the origin of the signal, *i.e.*, photothermal expansion of the materials for nanoIR as opposed to the absorbance of the material for FTIR. NanoIR signatures of non-embedded poplar cell wall layers were acquired (black

curves in Fig. 4), as well as spectra of the different embedded samples and corresponding pure resins (Fig 4a-d). Raw poplar clearly exhibited characteristic IR absorption bands of plant fibres attributed to cellulose (1372 and 1160cm^{-1} for instance), hemicellulose (1740 and 1372cm^{-1}) and lignin vibrations (1600, 1512 and 1320cm^{-1}) (Table 3) [38].

NanoIR spectra of the pure resins displayed the same bands as the ones observed in FTIR spectra (Table S2 and SI). Next we compared the spectra of the embedded sections to their respective pure resins and to raw poplar. The findings further confirmed the fact that Epon, LR White and Methacrylate diffuse differently in the cell wall. The fingerprint of poplar sections embedded in Epon contained bands from poplar and from the resin (Fig. 4a). In the range where Epon absorbs the most, such as between 1500 and 1600cm^{-1}, the characteristic bands of poplar were not discernible in the S2 layers. Findings confirmed that Epon penetrated the S2 layer, which is in agreement with the nanomechanical results. Given that when probing a large depth with Raman confocal spectroscopy, poplar bands were more clearly discernible, we infer that Epon is more concentrated close to the surface of the section, making it prominent in the nanoIR spectra. The signature of the S2 layers of the sample embedded in LR White displayed strong bands characteristic of poplar, especially in the region where the resin is not absorbing (Fig. 4). This is in contrast with a spectrum almost identical to the Methacrylate resin embedded section (Fig. 4c). No sign of poplar could be discerned in the Methacrylate-embedded S2 layers, which is in agreement with the Raman spectra and the nanomechanical results. After washing Methacrylate, the IR bands of the cell wall layers were resolved by nanoIR spectroscopy, though with some notable differences in band amplitude, suggesting that some resin remained at the surface of S2 layers (Fig. 4). The maximum position of the strongest band in the 1700 to 1800cm^{-1}, containing contributions of C=O vibrations from both the plant cell wall and Methacrylate, shifts from 1720cm^{-1} to 1740cm^{-1} after washing, suggesting the removal of the resin, whose C=O band peak is around 1736cm^{-1}. NanoIR findings confirm observations made from the Raman spectra. The appeal of nanoIR is its finer lateral resolution, which allows to probe the S1 layers, CML and CC. Epon bands were not discernible in S1

and CML, indicating a limited penetration beyond S2. However, signs of Epon could be observed in CC. For LR white, S1 and CML exhibit the characteristic bands of lignocellulosic fibres with spectra similar to the corresponding layers of the non-embedded poplar, showing that the diffusion of LR White is the lowest of the three resins considered in this study. No distinction between S2, S1, CML and CC could be made in presence of Methacrylate (Fig. 4). However, bands corresponding to neither the pure resin nor poplar were observed in the 1000-1100cm^{-1} range. Upon washing, the signature of poplar was retrieved. Next, nanoIR was used to map the distribution of resin in the cell walls, by monitoring the amplitude of the 1720cm^{-1} band observed for all 3 resins. Besides the aforementioned finding that the band shifts from 1720cm^{-1} to 1740cm^{-1} upon resin removal, the lumen (L) probed in all embedded sections exhibited a strong signal at that wavelength, which confirmed that it is resin-specific. In Fig. 4e, the Epon-embedded section exhibited a fairly constant amplitude, suggesting a uniform presence of the resin, in slight contrast with the nanoIR spectra. This could be due to the fact that Epon spectra did not change in the ~1720cm^{-1} unlike LR White and Methacrylate. Hence the chemical map for this case should be considered carefully. The variations observed at edges and layers interfaces could originate from an accumulation of resin or from an artefact due to the topography of the sample. For LR White, the amplitude of the photothermal expansion at the wavenumber monitored was significantly smaller in the cell wall layers than in the lumen (Fig. 4f), in good agreement with the low diffusion inferred from previous measurements.

The signal in CC, revealed a higher signal, which is consistent with the fact that the nanoIR spectrum of CC resembled the fingerprint of LR White. As a result, LR White diffusion or contamination of CC should be taken into account. Lastly, Fig. 4g confirms the presence of Methacrylate across the cell walls with constant amplitude in the Lumen (L), S2, S1, CML and CC. The resin seemed to have been mostly removed from the lumen after washing, although amplitude variations within the cell walls suggest that resin residues were still present (Fig. 4h).

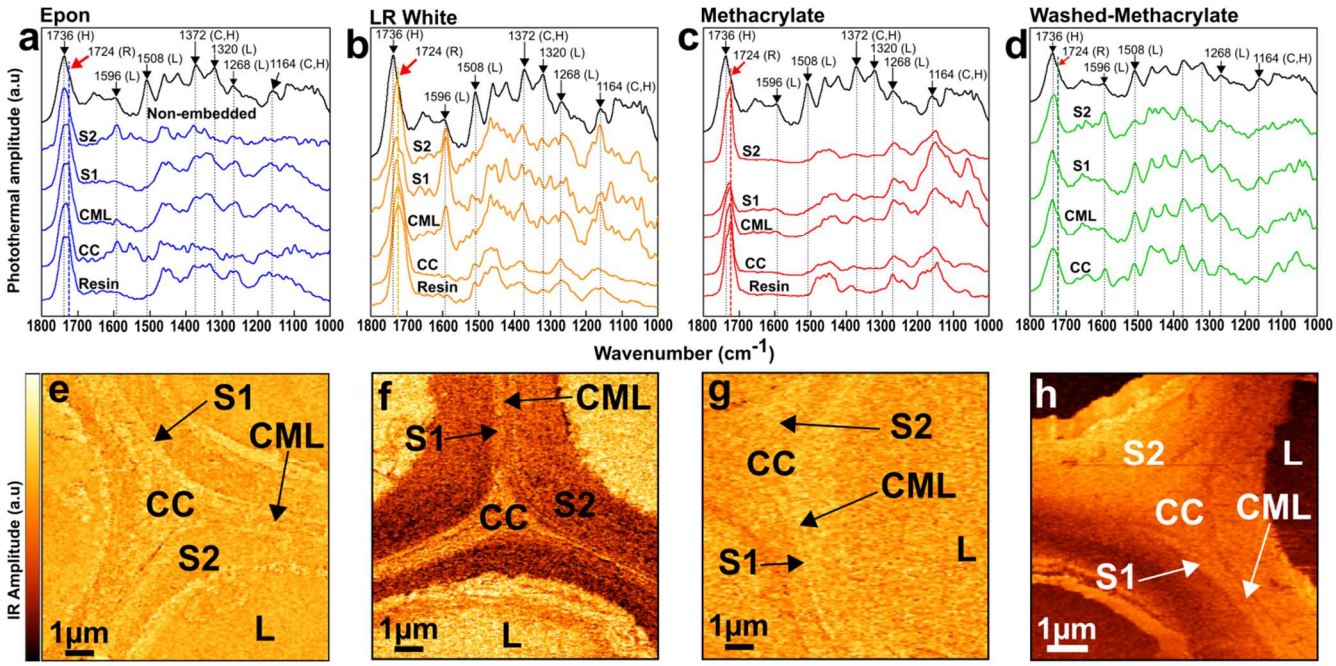

Figure 4. NanoIR spectra and corresponding IR mapping. (a-c) NanoIR spectra of S2, S1, CML and CC of poplar embedded in (a) Epon, (b) LR White, and (c) Methacrylate. Corresponding spectra of pure resins are shown. (d) NanoIR spectra of S2, S1 and CC of poplar section after washing Methacrylate. Black curves correspond to the nanoIR fingerprint of the non-embedded poplar. (e-h) NanoIR maps at 1720cm^{-1} (resin band indicated by the dotted black line on the spectra) of poplar embedded in (e) Epon, (f) LR White, (g) Methacrylate. (h) Corresponding map after Methacrylate washing.

4. Discussion

Well-established protocols for plant tissue preparation were originally developed for optical imaging and bioanalytical measurements. The lack of resolution and sensitivity of these techniques did not permit the detection of nanoscale residues and minute molecular interactions in the tissues. Today, the quest for highly efficient biofuel conversion schemes as well as for functional and tunable valorization, considering new computational and experimental powers for material by design, shed light on fundamental questions of the molecular interactions in complex plant tissues. In turn, treatments that could have been unchallenged for decades are being questioned. This is the case for embedding resins and their impact on plant cell wall layers. The multiscale and multifunctional measurements carried out in this work demonstrate that embedding can impact mechanical and chemical traits of the cell wall

layers, even with commonly used resins. In the literature, the effect of resin on the mechanical properties of wood fibre reinforced composites has already been studied at macroscale using tensile test [39]. They reported that filling the lumen of sisal fibres with epoxy resin led to an increase of the tensile modulus. At the cell wall level, contradictory results have been reported regarding the effect of resin on the mechanical properties of S2 layer probed with nanoindentation. Hepworth et al. observed cell wall swelling after using an epoxy resin (S.P. Systems Ampreg 26) diluted with ethyl alcohol, attributing resin diffusion to the increase in stiffness measurements in the fibres [21]. Meng et al. also found that Spurr's resin, a low viscosity epoxy, leads to higher modulus of plant fibres [40]. On the other hand, elastic modulus and hardness did not vary significantly following embedding of freshly cut southern pine (Pinus spp.) sapwood in Spurr's epoxy prior to exposure to brown rot to produce decayed wood cell walls according to Kim et al. [22]. Given the lack of chemical characterization and the limited resolution of nanoindentation, a detailed understanding of the interaction between resins and plant cell walls could not be drawn from these studies. By taking advantage of recent advances in multiscale platforms, we unveiled here the mechanical and chemical impact of Epon, LR White and Methacrylate on the different cell wall layers of poplar.

The reduced IM in S2 layer of LR white poplar measured by nanoindentation was similar to non-embedded sample while the one obtained by PFQNM was slightly higher though still within standard variation. Accordingly, LR White exhibits low diffusion in S2 layer as shown by Raman and nanoinfrared analysis. In contrast, the presence of Epon and Methacrylate was shown in the S2 layer, with a more pronounced signal for Methacrylate. As a result, the increase in IM observed in the S2 layer evaluated by nanoindentation and AFM PFQNM is likely due to the elastic constraint exerted by the resin on the polymer architecture of the layers. It is also possible that the resin present in the lumen can reduce the buckling of the cell wall, as they naturally would under a nanoindentation load, leading to an increase of the indentation modulus. The higher reduced IM is indicative of a strong interaction between the resin and the plant cell walls, leading to a strengthening of the different layers. It has been already

reported that epoxy resins can penetrate the plant cell walls leading to an increase of their mechanical properties [21]. The polymerization process of this resin could also explain the increase of the reduced IM of poplar embedded in Epon. Indeed, Epon belongs to the family of epoxy, which are resins that create cross links between their macromolecular chains leading to very stable networks [41].

Further exploration with PFQNM revealed local behaviors that could not be detected by nanoindentation. Notably, when probing a smaller volume of the tissues, a reduced IM about 7GPa was measured for the Methacrylate-embedded poplar, which divulges for the first time that sectioning a sample embedded with Methacrylate smears a thin layer of resin at the surface of the sample. This explains the soft aspect of the surface (~7GPa) when probed with the small indent in PFQNM but the larger reduced IM (~22GPa) when the indentation volume was beyond the thickness of the film covering the surface. Washing Methacrylate led to the retrieval of IR and Raman bands corresponding to S2 poplar cell wall, although residues remained. Nanoindentation confirmed the removal of the resin upon washing. However, PFQNM results suggested that strong interactions between the cell walls and Methacrylate occurred near the surface evidenced by a slight increase in reduced IM. Thus, the constraints imposed by Methacrylate would be released by washing, allowing the molecular architecture of the layers to retrieve a structure in volume close to that of the original non-embedded S2 wall layer. The process is not fully reversible based on nanoscale findings as shown by the higher value of reduced IM of the S2 layer after washing compared to non-embedded sample.

The nanoscale resolution of PFQNM and nanoIR made it possible to probe the properties of S1, CML, and CC. PFQNM results suggest that each resin has a different impact on poplar plant cell walls. Regarding the nanoIR spectra, Epon seemed to diffuse in layers beyond S2, especially in the S1 and the CC with small impact on the IM values. NanoIR spectra and reduced IM indicate that LR White diffusion is not significant in S1, CML and CC. Methacrylate, on the other hand, affected all layers as evidenced by the low reduced IM values and absence of poplar signature in the nanoIR spectra. Washing the Methacrylate allowed to recover IM values in the S1, CML and CC layers similar to the non-

embedded poplar, but with higher IM for the S2 layer. This difference could be explain by the fact that, although S1 and S2 are mainly composed of cellulose microfibrils, lignin and hemicellulose, the cellulose microfibrils angle (MFA) is closer to the cell axis in S2 (15.8° ± 0.1° for poplar) [31] than in S1 (typically 70-90°) [42]. It was previously inferred that penetration of resins preferentially occurs in the longitudinal axis of the cells [19], i.e., in S2. The use of alcohol and/or acetone for the initial dehydration steps involved in the preparation of the sections could also affect the porosity and the supramolecular architecture of the plant cell wall as water is removed [17]. This step has not yet been characterized at the nanoscale to the best of our knowledge. Here, sections embedded in LR White and Methacrylate underwent the same dehydration steps. Nonetheless, despite soaking in the resin for several hours and using vacuum to force the penetration of the solution prior to polymerization, the penetration of LR White, a polyhydroxy-aromatic acrylic resin, through the micro- and nano-pores of the plant seems more challenging than for Methacrylate. This is probably due to the presence of the aromatic groups in LR White while Methacrylate only possesses linear chains without aromatic groups. The diffusion of the resins can be related to physicochemical characteristics (molecular weight, shape of the molecule, viscosity) which may not be readily available for proprietary resins such as LR white. Furthermore, it has been reported that chemical groups of resins such as urea-formaldehyde and 1,3-dimethylol-4,5-dihydroxyethyleneurea (DMDHEU) can likely react with carbonyl (C=O) and hydroxyl (−OH) groups of the wood polymers covalently [43]. This could explain the difference in diffusion into the cell wall of the resins used for this study. Further studies on penetration and diffusion of resins could benefit the development of natural fibres composite deserving various application fields (Zhang, Z., et al. (2020)) [44].

5. Conclusions

Our results demonstrate that the use of resin embedding media to characterize plant cell walls at the nanoscale, although helpful to avoid damages, can lead to misleading analyses. Care should be taken when using resin embedding media. Effects on the non-embedded mechanical properties of plant fibres

of the resins can be unnoticeable at the macro- and microscale, but significant at the nanoscale. For poplar, LR White would circumvent major diffusion or contamination of the surface. Non-diffusing resin should be preferred to the option of washing after embedding, as seen from residues and mechanical changes observed after washing Methacrylate. Our investigations altogether highlight the importance of multiscale analysis to develop a clearer appreciation of heterogeneous three dimensional systems such as plant fibres, and the need for new and refined protocols to circumvent diffusion and potential chemical modifications in manipulations of biological tissues.

Conflicts of interest

There are no conflicts to declare.

Acknowledgements

MM and BC thank the Nano'Mat platform of the University of Reims Champagne Ardenne funded through the Region Grand Est, the DDRT Grand Est and the FEDER program. RC acknowledges the support of the Grand Est Region for cofounding of the doctoral grant. MM thanks the Fulbright program for his scholar fellowship. LT acknowledges the shared facilities of the University of Central Florida.

Funding

This work was supported by ANR PRCI IntoS2 program (grant n° ANR-18-CE93-0007-02), and the Southeastern Regional Sun Grant Center at the University of Tennessee through a grant provided by the U.S. Department of Agriculture (award number 2014-38502-22598).

Author contributions

LT, BC, and MM designed the study. RC, LT, V A-B, BC, and MM analyzed the results, treated the data and wrote the manuscript. RC, MS and KL performed and analyzed the Raman data. RC and SP performed the nanoindentation experiments. NB, RC, and MM performed the nanoIR measurements. RC performed and analyzed the PFQNM experiments. All authors read and approved the final manuscript.

References

[1] B. Madsen, E.K. Gamstedt, Wood versus plant fibers: Similarities and differences in composite applications, Adv. Mater. Sci. Eng. 2013 (2013) 1-14. https://doi.org/10.1155/2013/564346
[2] V.K. Thakur, M.K. Thakur, R.K. Gupta, Review: Raw natural fiber–based polymer composites, Int. J. polym. Anal. Ch. 19 (2014) 256-271. https://doi.org/10.1080/1023666X.2014.880016
[3] R.A. Burton, M.J. Gidley, G.B. Fincher, Heterogeneity in the chemistry, structure and function of plant cell walls, Nat. Chem. Biol. 6(10) (2010) 724-732. https://doi.org/10.1038/nchembio.439
[4] L. Salmén, I. Burgert, Cell wall features with regard to mechanical performance. A review COST Action E35 2004–2008: Wood machining – micromechanics and fracture, Holzforschung 63 (2009) 121-129. https://doi.org/10.1515/HF.2009.011
[5] D.J. Cosgrove, Expansive growth of plant cell walls, Plant Physiol. Bioch. 38 (2000) 109–124. https://doi.org/10.1016/S0981-9428(00)00164-9
[6] N. Gierlinger, New insights into plant cell walls by vibrational microspectroscopy, Appl. Spectrosc. Rev. 53(7) (2018) 517-551. https://doi.org/10.1080/05704928.2017.1363052
[7] U.P. Agarwal, Raman imaging to investigate ultrastructure and composition of plant cell walls: Distribution of lignin and cellulose in black spruce wood (Picea mariana), Planta 224(5) (2006) 1141-1153. https://doi.org/10.1007/s00425-006-0295-z
[8] L. Salmén, J.S. Stevanic, A.-M. Olsson, Contribution of lignin to the strength properties in wood fibres studied by dynamic FTIR spectroscopy and dynamic mechanical analysis (DMA), Holzforschung 70(12) (2016) 1155-1163. https://doi.org/10.1515/hf-2016-0050
[9] A.-M. Olsson, I. Bjurhager, L. Gerber, B. Sundberg, L. Salmén, Ultra-structural organisation of cell wall polymers in normal and tension wood of aspen revealed by polarisation FTIR microspectroscopy, Planta 233(6) (2011) 1277-1286. https://doi.org/10.1007/s00425-011-1384-1
[10] H. Van As, T. Scheenen, F.J. Vergeldt, MRI of intact plants, Photosynth Res 102(2-3) (2009) 213-222. https://doi.org/10.1007/s11120-009-9486-3
[11] J.E. Jakes, C.R. Frihart, J.F. Beecher, R.J. Moon, P.J. Resto, Z.H. Melgarejo, O.M. Suárez, H. Baumgart, A.A. Elmustafa, D.S. Stone, Nanoindentation near the edge, J. Mater. Res. 24(3) (2011) 1016-1031. https://doi.org/10.1557/jmr.2009.0076
[12] R. Wimmer, B.N. Lucas, W.C. Oliver, T.Y. Tsui, Longitudinal hardness and Young's modulus of spruce tracheid secondary walls using nanoindentation technique, Wood Science and Technology 31(2) (1997) 131-141. https://doi.org/10.1007/BF00705928

[13] S. Piqueras, S. Füchtner, R. Rocha de Oliveira, A. Gómez-Sánchez, S. Jelavić, T. Keplinger, A. de Juan, L.G. Thygesen, Understanding the Formation of Heartwood in Larch Using Synchrotron Infrared Imaging Combined With Multivariate Analysis and Atomic Force Microscope Infrared Spectroscopy, Front. Plant. Sci. 10(1701) (2020). https://doi.org/10.3389/fpls.2019.01701
[14] L. Tetard, A. Passian, R.H. Farahi, T. Thundat, B.H. Davison, Opto-nanomechanical spectroscopic material characterization, Nature Nanotechnology 10(10) (2015) 870-877. https://doi.org/10.1038/nnano.2015.168
[15] A. Bourmaud, J. Malvestio, N. Lenoir, D. Siniscalco, A. Habrant, A. King, D. Legland, C. Baley, J. Beaugrand, Exploring the mechanical performance and in-planta architecture of secondary hemp fibres, Ind. Crops Prod. 108 (2017) 1-5. https://doi.org/10.1016/j.indcrop.2017.06.010
[16] A.M. Glauert, G.E. Rogers, R.H. Glauert, A new embedding medium for electron microscopy, Nature 178(4537) (1956) 803-803. https://doi.org/10.1038/178803a0
[17] B.Q. Huang, E.C. Yeung, Chemical and physical fixation of cells and tissues: An overview, in: S.C. Yeung E., Sumner M., Huang B. (Ed.), Plant Microtechniques and Protocols, Springer, Cham2015, pp. 23-43.
[18] C.G. Hunt, J.E. Jakes, W. Grigsby, Evaluation of adhesive penetration of wood fibre by nanoindentation and microscopy, BIOCOMP 2010 : 10th Pacific Rim Bio-Based Composites Symposium : 5-8 October 2010, 2010.
[19] F.A. Kamke, J.N. Lee, Adhesive penetration in wood—A review, Wood Fiber Sci. 39 (2007) 205–220.
[20] L. Wagner, T.K. Bader, K. de Borst, Nanoindentation of wood cell walls: effects of sample preparation and indentation protocol, J. Mater. Sci. 49 (2014) 94-102. https://doi.org/10.1007/s10853-013-7680-3
[21] D.G. Hepworth, J.F.V. Vincent, G. Jeronimidis, D.M. Bruce, The penetration of epoxy resin into plant fibre cell walls increases the stiffness of plant fibre composites, Compos. Part A. Appl. Sci. 31 (2000) 599–601. https://doi.org/10.1016/S1359-835X(99)00097-4
[22] J.-W. Kim, D.P. Harper, A.M. Taylor, Technical note: effect of epoxy embedment on micromechanical properties of brown-rot-decayed wood cell walls assessed with nanoindentation, Wood Fiber Sci. 44(1) (2012) 103-107.
[23] L. Muraille, V. Aguié-Béghin, B. Chabbert, M. Molinari, Bioinspired lignocellulosic films to understand the mechanical properties of lignified plant cell walls at nanoscale, *Sci. Rep.* 7 (2017) 44065. https://doi.org/10.1038/srep44065

[24] D. Ren, H. Wang, Z. Yu, H. Wang, Y. Yu, Mechanical imaging of bamboo fiber cell walls and their composites by means of peakforce quantitative nanomechanics (PQNM) technique, Holzforschung 69(8) (2015) 975-984. https://doi.org/10.1515/hf-2014-0237
[25] A. Dazzi, C.B. Prater, Q. Hu, D.B. Chase, J.F. Rabolt, C. Marcott, AFM–IR: Combining atomic force microscopy and infrared spectroscopy for nanoscale chemical characterization, Appl. Spectrosc. 66 (2012) 1365–1384. https://doi.org/10.1366/12-06804
[26] J.E. Jakes, C.R. Frihart, J.F. Beecher, R.J. Moon, D.S. Stone, Experimental method to account for structural compliance in nanoindentation measurements, J. Mater. Res. 23(4) (2011) 1113-1127. https://doi.org/10.1557/jmr.2008.0131
[27] M. Troyon, S. Lafaye, About the importance of introducing a correction factor in the Sneddon relationship for nanoindentation measurements, Philosophical Magazine 86(33-35) (2006) 5299-5307. https://doi.org/10.1080/14786430600606834
[28] W.C. Oliver, G.M. Pharr, An improved technique for determining hardness and elastic modulus using load and displacement sensing indentation experiments, J. Mater. Res. 7(6) (1992) 1564-1583. https://doi.org/10.1557/JMR.1992.1564
[29] J.E. Sader, J.W.M. Chon, P. Mulvaney, Calibration of rectangular atomic force microscope cantilevers, Rev. Sci. Instrum. 70(10) (1999) 3967-3969. https://doi.org/10.1063/1.1150021
[30] B.V. Derjaguin, V.M. Muller, Y.P. Toporov, Effect of contact deformations on the adhesion of particles, J. Colloid. Interf. Sci. 53(2) (1975) 314-326. https://doi.org/10.1016/0021-9797(75)90018-1
[31] Y. Wu, S. Wang, D. Zhou, C. Xing, Y. Zhang, Use of nanoindentation and silviscan to determine the mechanical properties of 10 hardwood species, Wood Fiber Sci. 41 (2009) 64–73.
[32] Y. Zhang, Y.-J. Meng, Y. Wu, S.-Q. Wang, G.-B. Du, H. Jiang, Z.-B. Zhou, Effect of enzyme treatment on the mechanical properties of wood cell walls by nanoindentation, BioResources 7 (2012) 2249-2259. https://doi.org/10.15376/biores.7.2.2249-2259
[33] L. Bertinetti, U.D. Hangen, M. Eder, P. Leibner, P. Fratzl, I. Zlotnikov, Characterizing moisture-dependent mechanical properties of organic materials: humidity-controlled static and dynamic nanoindentation of wood cell walls, Philosophical Magazine 95(16-18) (2015) 1992-1998. https://doi.org/10.1080/14786435.2014.920544
[34] R. Coste, M. Pernes, L. Tetard, M. Molinari, B. Chabbert, Effect of the interplay of composition and environmental humidity on the nanomechanical properties of hemp fibers, ACS Sustain. Chem. Eng. (2020). https://doi.org/10.1021/acssuschemeng.0c00566

[35] N. Gierlinger, M. Schwanninger, Chemical imaging of poplar wood cell walls by confocal Raman microscopy, Plant Physiol. 140(4) (2006) 1246-1254. https://doi.org/10.1104/pp.105.066993
[36] U.P. Agarwal, J.D. McSweeny, S.A. Ralph, FT–Raman investigation of milled-wood lignins: Softwood, hardwood, and chemically modified black spruce lignins, J. Wood. Chem. Technol. 31(4) (2011) 324-344. https://doi.org/10.1080/02773813.2011.562338
[37] A. Dazzi, C.B. Prater, AFM-IR: Technology and Applications in Nanoscale Infrared Spectroscopy and Chemical Imaging, Chemical Reviews 117(7) (2017) 5146-5173. https://doi.org/10.1021/acs.chemrev.6b00448
[38] N. Gierlinger, L. Goswami, M. Schmidt, I. Burgert, C. Coutand, T. Rogge, M. Schwanninger, In Situ FT-IR Microscopic Study on Enzymatic Treatment of Poplar Wood Cross-Sections, Biomacromolecules 9(8) (2008) 2194-2201. https://doi.org/10.1021/bm800300b
[39] Y. Li, H. Ma, Y. Shen, Q. Li, Z. Zheng, Effects of resin inside fiber lumen on the mechanical properties of sisal fiber reinforced composites, Compos. Sci. Technol. 108 (2015) 32-40. https://doi.org/10.1016/j.compscitech.2015.01.003
[40] Y. Meng, S. Wang, Z. Cai, T.M. Young, G. Du, Y. Li, A novel sample preparation method to avoid influence of embedding medium during nano-indentation, Appl. Phys. A-Mater. 110 (2013) 361-369. https://doi.org/10.1007/s00339-012-7123-z
[41] R. Unger, U. Braun, J. Fankhänel, B. Daum, B. Arash, R. Rolfes, Molecular modelling of epoxy resin crosslinking experimentally validated by near-infrared spectroscopy, Computational Materials Science 161 (2019) 223-235. https://doi.org/10.1016/j.commatsci.2019.01.054
[42] L. Donaldson, Microfibril angle: Measurement, variation and relationships – a review, IAWA J. 29(4) (2008) 345-386. https://doi.org/10.1163/22941932-90000192
[43] X. Han, X. Miao, X. Zheng, L. Xing, J. Pu, Chemical modification by impregnation of poplar wood with functional composite modifier, BioResources 10 (2015) 5203-5214. https://doi.org/10.15376/biores.10.3.5203-5214
[44] Z. Zhang, S. Cai, Y. Li, Z. Wang, Y. Long, T. Yu, Y. Shen, High performances of plant fiber reinforced composites—A new insight from hierarchical microstructures, Compos. Sci. Technol. 194 (2020) 108151. https://doi.org/10.1016/j.compscitech.2020.108151

Mechanical properties ⟷ Resin distribution

Poplar Fiber

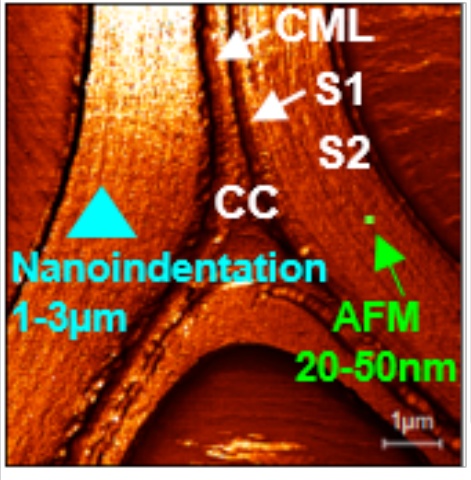

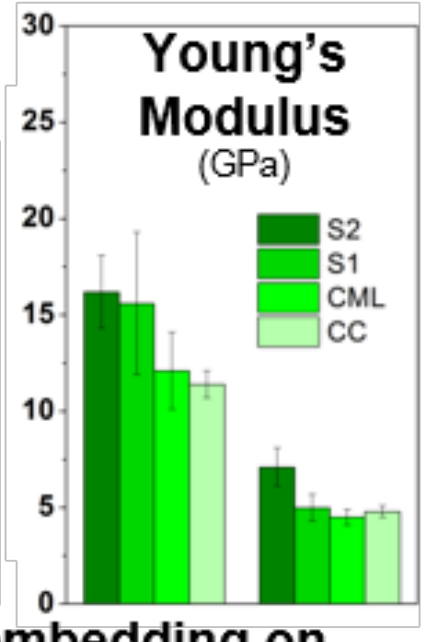

Impact of the embedding on nanomechanical properties

NanoIR spectra